FAST AND SLOW SUBSYSTEMS FOR A CONTINUUM MODEL OF BURSTING ACTIVITY IN THE PANCREATIC ISLET*

M. PERNAROWSKI†

Abstract. A simple model for the bursting electrical activity of individual pancreatic β-cells is introduced. Using the model, a continuum model for collections (islets) of large numbers of such cells is then analyzed using asymptotic methods, linear stability techniques and monotone methods. When the coupling strength D is large, fast and slow subsystems for the continuum model are shown to be the same as those for the single cell if the slow variables are replaced by their spatial average. It is demonstrated that fast variables can synchronize while the slow variables simultaneously exhibit nonsynchronous behavior. Lastly, spatial inhomogeneities in slow subsystem parameters are shown to inactivate the islet. It is demonstrated that if a sufficient fraction of cells are inactive, the average value of the slow variables can be decreased significantly.

Key words. bursting, coupled oscillators, pancreatic β-cells, continuum model

AMS(MOS) subject classifications. 34A, 34C, 39A, 65N40, 92C

1. Introduction. The pancreas consists of millions of islets. Each islet is surrounded by a reticular membrane and contains several thousand endocrine cells. The insulin secreting β-cells account for 60-80% of all the cells in the islet. In most experiments, islets are removed from mice and electrical measurements are made at room temperature. For these experiments, bursting electrical activity (BEA) is observed in β-cells which are still intact in the islets ([6],[7],[16],[24]). At elevated temperatures (30° C), bursting was observed in β-cells which were isolated from the islet [30]. In other experiments at room temperature using different measuring techniques, isolated β-cells exhibit depolarization and irregular spiking but do not burst [10]. The variability in such experimental results has raised many questions about the contrasting behavior of isolated cells and cells in intact islets.

It is known that β-cells are electrically coupled to each other via gap junction channels [18]. This fact has been used in recents models to examine the behavior of β-cells in intact islets. Smolen et al [31] have used an islet model to demonstrate how cell heterogeneity could explain why cells burst when electrically coupled but do not burst when isolated from the islet. In addition to this issue, there are the issues of synchronization and the dependence of islet activity on glucose concentration. At low glucose concentrations intact cells do not burst. At intermediate concentrations some studies [1] indicate that a fraction of the cells burst while at higher concentrations all cells appear to burst in synchrony ([14],[15])

Dimensional models of individual β-cell electrical activity ([3],[4],[5],[12],[22],[29], [2]) are described by:

$$C_m \frac{dv}{dt} = -\sum_X I_X(v, w, \vec{c}) \ , \tag{1}$$

$$\frac{dw}{dt} = \frac{w_\infty(v, \vec{c}) - w}{\tau(v, \vec{c})} \ , \tag{2}$$

* This work was supported by the National Science Foundation grants OSR-93-50-546 and DMS-94-04-521

† Department of Mathematical Sciences, Montana State University, Bozeman, Montana 59717. Email: pernarow@math.montana.edu

$$\frac{d\vec{c}}{dt} = \varepsilon\vec{h}(v,w,\vec{c}) \quad ,\vec{c}\in \mathbb{R}^K \quad , \tag{3}$$

where v is the membrane potential, I_X is the membrane ionic current through channels of type X, w is a channel activation parameter for the voltage-gated potassium channel, C_m is the total cell capacitance, and ε is a small parameter. The variables $\vec{c}$ are often concentrations of agents which regulate the BEA (bursting electrical activity) such as intracellular calcium, concentration of calcium in the endoplasmic reticulum and ADP. Specific forms of the functions defining (1)-(3) depend on what assumptions were made to derive the model equations.

In an islet model, each β-cell consists of varying numbers of channels of each type (i.e., voltage-gated calcium, calcium-activated potassium, ...) and each individual channel has its own conductance. The islet occupies a region Ω in space and the m-th β-cell is located at $\vec{x}_m = (x_m, y_m, z_m) \in \Omega$. The current through all gap junctions connecting cells m and n is:

$$I_{m,n} = g_{m,n}(v_m - v_n) \quad , \tag{4}$$

where v_m and v_n are the membrane potentials of cells m and n, respectively, and $g_{m,n}$ is the net conductance of all such gap junctions connecting the two cells. If cells m and n are not coupled, $g_{m,n} = 0$. Thus, for the m-th cell ($m = 1, 2, \ldots M$)

$$C_m\frac{dv_m}{dt} = -\sum_X I_X(v_m, w_m, c_m) - \sum_{n=1}^{M} g_{m,n}(v_m - v_n) \ , \tag{5}$$

$$\frac{dw_m}{dt} = \frac{w_\infty(v_m, c_m) - w_m}{\tau(v_m, c_m)} \ , \tag{6}$$

$$\frac{dc_m}{dt} = \varepsilon h(v_m, w_m, c_m) \ , \ \varepsilon \ll 1 \ . \tag{7}$$

There have been a few attempts to analyze models of the form (5) – (7). In numerical simulations, Sherman and Rinzel [27, 28] discovered that for different coupling conductances a system of two coupled (identical) bursters can exhibit both in-phase (synchronized) and out of phase solutions. A more recent study by Sherman [32] explained this phenomena using a generalization of the fast-slow subsystem analysis used to explain the single cell bursting cycle [19, 23]. There, the multiple branches of critical points and periodic solutions of the fast subsystem complicate the dynamics.

As new experimental evidence has become available, the assumptions defining single cell models (1)-(3) have changed. In addition to this evolution, it is not understood what effect the magnitude of $g_{m,n}$ has on the islet electrical behavior in (5)-(7). To illustrate this issue, we estimate the nondimensional coupling conductance γ_c, for homogenous coupling, i.e., $g_{m,n} = g_c$ for all m and n. The dimensional coupling conductance g_c has been measured in isolated β-cell pairs by Perez-Armendariz et al [18] as $g_c = 215 \pm 110pS$. Following the nondimensionalization of the SRK model [29] presented in Pernarowski et al [20]

$$\gamma_c = \frac{g_c\bar{\tau}_n}{C_m} \quad , \tag{8}$$

where $\bar{\tau}_n$ is a characteristic time associated with the voltage-gating in the potassium channels. Using values from a recent model [2] ($\bar{\tau}_n = 4.86$ msec, $C_m = 6158$ fF)

yields $\gamma_c = 0.174 \pm 0.082$. Not only is there a large variability in this value of γ_c but it seems somewhat low to explain the observed synchrony in the islet electrical behavior. However, the value of g_c measured by Perez-Armendariz et al [18] is for cell pairs dissociated from the islet and not for cells in intact islets. The synchronous electrical activity measured in intact islets suggest that appropriate modelling values for g_c may be higher. These issues and facts form the motivation for studying continuum islet model behavior. The bulk of this paper addresses only issues associated with higher coupling strengths.

First, a single cell model is developed in section 2 and a brief description of the fast-slow subsystem description of square-wave bursting is then given in section 3. The fast-slow subsystem explanation due to Rinzel [23] is valid only for certain slow subsystem parameters. For some parameter values, the same system exhibits stationary behavior. In section 4, the dependence of existence and stability of equilibria on slow subsystem parameters is examined in the single cell model. In a two-dimensional slow subsystem parameter space, two regions are determined where the model exhibits stable stationary and bursting behaviors.

In section 5, a continuum model for islet electrical activity is introduced. Gap junction coupling in the three dimensional islet model (5)-(7) is replaced by a spatially nonhomogeneous diffusion term. For large coupling strength D, an asymptotic analysis yields fast and slow subsystems analagous to those of the single cell model. In section 7, these subsystems are shown to be the same as their single cell counterparts when the slow variables are replaced by their spatial averages. Also, the introduction of the diffusive coupling is shown not to affect the steady state structure of the model. In section 6, monotone methods are used to show that for all diffusion strengths the continuum (partial differential equation) model possesses only those equilibria present in the single cell model. Furthermore, slow parameter dependence of both stability and existence of these equilibria are shown to be identical to that obtained in section 4.

Lastly, in section 8, a spatially heterogeneous continuum model is examined. The heterogeneity considered introduces populations of active and inactive cells in the islet. When decoupled from other cells, inactive and active cells exhibit stationary and bursting behavior, respectively. A rederivation of fast and slow subsystems for this model reveals that islet electrical activity can be stationary if only a relatively small fraction of cells are inactive. Moreover, this stationary behavior yields lower average values for the slow variables. Physiologically, these lowered values are known to decrease insulin production.

2. Single cell model. In this section, we define an analog model for β-cell models which can be transformed into systems of the form:

$$\frac{du}{dt} = f(u) - w - k(c) \quad , \tag{9}$$

$$\frac{dw}{dt} = \frac{1}{\tau_w(u)}(w_\infty(u) - w) \quad , \tag{10}$$

$$\frac{dc}{dt} = \varepsilon(h(u) - c) \quad , \tag{11}$$

where we note that $\varepsilon \ll 1$ is a small positive parameter.

By differentiating (9) in t and using (9)-(11) to eliminate w, (9)-(10) can be written in the Liénard form:

$$\frac{d^2u}{dt^2} + F(u)\frac{du}{dt} + G(u,c) = -\varepsilon k'(c)(h(u) - c) \quad , \tag{12}$$

where

$$F(u) = \frac{1}{\tau_w(u)} - f'(u) \quad , \tag{13}$$

$$G(u,c) = \frac{1}{\tau_w(u)}(w_\infty(u) + k(c) - f(u)) \quad . \tag{14}$$

The dependence of (11)-(12) on parameter values occurring solely in the fast subsystem ($\varepsilon = 0$) has been studied in detail in ([19],[8]) for a simple polynomial model. The functions defining that model are

$$F(u) = a((u - \hat{u})^2 - \eta^2) \quad , \tag{15}$$

$$G(u,c) = c + u^3 - 3(u + 1) \quad , \tag{16}$$

$$h(u) = \beta(u - u_\beta) \quad . \tag{17}$$

For different parameter values for $\vec{\lambda} = (a, \eta, \hat{u}, \beta, u_\beta, \varepsilon)$ the model defined by (11)-(12) and (15)-(17) exhibits a variety of different oscillatory behaviors. For a bounded region in fast parameter space $\vec{\lambda}_f = (a, \eta, \hat{u})$, the model exhibits square-wave bursting analogous to BEA in the pancreatic β-cell. One such set of parameter values is specified in [19]

$$a = \frac{1}{4} \quad , \eta = \frac{3}{4} \quad , \hat{u} = \frac{3}{2} \quad , \beta = 4 \quad , u_\beta = -0.954 \quad , \varepsilon = 0.0025 \quad . \tag{18}$$

A bifurcation analysis of the single cell model is best accomplished when the system is posed in the form (11)-(12) since homoclinic points can be found explicitly using Melnikov techniques (see [19]). However, the form (9)-(11) is needed to make a more direct correspondence to the coupled β-cell models (5)-(7).

Therefore, we proceed to determine functions $f(u)$, $k(c)$ and $w_\infty(u)$ to which $F(u)$ and $G(u,c)$ correspond. To make this connection between (9)-(11) and (11)-(12), we assume the relaxation time approximation

$$\tau_w(u) = \bar{\tau} \quad , \tag{19}$$

for some constant $\bar{\tau}$. This approximation was used in [20] as an approximation for the SRK model. In [21], it was shown that the silent phase duration is unaffected to leading-order by $\tau_w(u)$ but that the value of $\bar{\tau}$ used in the approximation significantly changed the leading-order active duration. Nevertheless, the overall qualitative features of the bursting cycle remains intact for a large range of $\bar{\tau}$ values.

Using (15) and (19) in (13) we deduce that $f(u)$ is cubic in u:

$$f(u) = f_3u^3 + f_2u^2 + f_1u + f_0 \quad , \tag{20}$$

$$f_3 = -\frac{a}{3} \quad , \tag{21}$$

$$f_2 = a\hat{u} \quad , \tag{22}$$

$$f_1 = \frac{1}{\bar{\tau}} - a(\hat{u}^2 - \eta^2) \quad , \tag{23}$$

where f_0 is an arbitrary constant. Equating (16) and (14), and using (20)-(23) we deduce:

$$k(c) = \bar{\tau}c \quad , \tag{24}$$

$$w_\infty(u) = \omega_3 u^3 + \omega_2 u^2 + \omega_1 u + \omega_0 \quad , \tag{25}$$

$$\omega_3 = f_3 + \bar{\tau} = \bar{\tau} - \frac{a}{3} \quad , \tag{26}$$

$$\omega_2 = f_2 \quad , \tag{27}$$

$$\omega_1 = f_1 - 3\bar{\tau} = \frac{1}{\bar{\tau}} - a(\hat{u}^2 - \eta^2) - 3\bar{\tau} \quad , \tag{28}$$

$$\omega_0 = f_0 - 3\bar{\tau} \quad . \tag{29}$$

We note that f_0 represents a shift in w since (9)-(11) is invariant under the transformation $W = w - f_0$. Thus, without loss of generality, we may set

$$f_0 = 0. \tag{30}$$

For the remainder of the paper we use the single cell model defined by (9)-(11) with functions defined via (19)-(30), $\bar{\tau} = 1$ and the parameter values stipulated in (18).

3. Fast-slow subsystems for single cell model. Under certain hypotheses, Terman [33] has shown that systems of the form (9)-(11) possess a periodic (bursting) solution. Terman's existence proof is a dynamical systems formalization of the fast-slow subsystem explanation of square-wave bursting [19, 23]. Here we briefly summarize the fast-slow subsystem description due to Rinzel [23], and discuss some global bifurcations due to changing parameter values in the slow subsystem.

On the "fast" t time scale the solution behavior of (9)-(11) is governed by the fast subsystem obtained by letting $\varepsilon = 0$

$$\frac{du}{dt} = f(u) - w - c \quad , \tag{31}$$

$$\frac{dw}{dt} = \frac{1}{\tau_w(u)}(w_\infty(u) - w) \quad , \tag{32}$$

where c is a parameter.

The bifurcation diagram of this system is generated using AUTO [9] in Figure 1. Stable limit cycles eminate from a Hopf point at $c = c_{HB}$ and terminate at a homoclinic point at $c = c_{HC}$. Equilibria of the fast subsystem lie on $c = g(u)$:

$$g(u) = f(u) - w_\infty(u) = -u^3 + 3(u+1) \quad . \tag{33}$$

For $c_m < c < c_M$, the lower, middle and upper branch equilibria are stable, saddles and unstable spirals, respectively [19]. Projected on this figure is the numerical

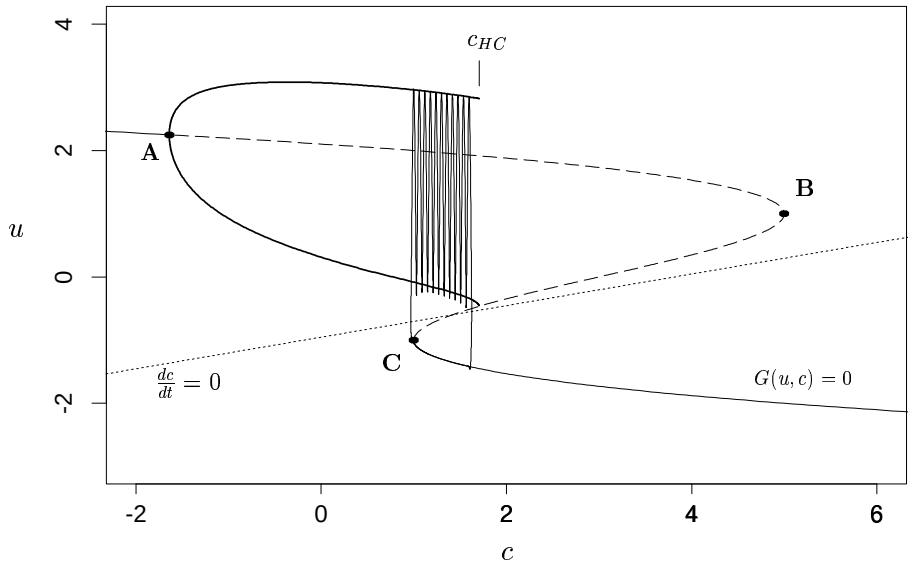

FIG. 1. *Solution $(u(t), w(t), c(t))$ of a single cell projected onto fast subsystem bifurcation diagram. Active phase oscillations lie near a stable (solid) limit cycle branch eminating from a Hopf point A. The silent phase solution lies near the stable lower branch of the $c = g(u)$ manifold. Points B and C have coordinates $(c_M, u_M) = (5, 1)$ and $(c_m, u_m) = (1, -1)$, respectively.*

solution of (9)-(11). The high frequency oscillations of $u(t)$ which characterize the active phase of the bursting cycle are seen to lie close to the manifold formed by the stable periodic solutions of the fast subsystem.

In the silent phase, both $u(t)$ and $c(t)$ evolve on a slow $\tilde{t} = \varepsilon t, \varepsilon \ll 1$, time scale. The leading-order problem for this time scale (slow subsystem) is

$$c = g(u), \tag{34}$$

$$\frac{dc}{d\tilde{t}} = h(u) - c. \tag{35}$$

Differentiating (34) in $\tilde{t}$ and then using (34)-(35) to eliminate c yields

$$\frac{du}{d\tilde{t}} = \frac{h(u) - g(u)}{g'(u)} \quad . \tag{36}$$

Thus, in the silent phase, solutions of (9)-(11) lie close to the stable (lower) branch of the $c = g(u)$ manifold with dynamics determined from (35)-(36). Below the $\frac{dc}{dt} = 0$ nullcline (dashed line) c decreases. Above this nullcline (active phase) c increases. Transitions between phases occur (to leading-order) at the left knee of $c = g(u)$ and at the homoclinic point of the fast subsystem. Each time a transition occurs, the sign of $\frac{dc}{dt}$ changes explaining the continued alternation of active and silent phases which characterize the (square-wave) bursting oscillations.

4. Slow subsystem bifurcations in the single cell model. It is important to emphasize that square-wave bursting solutions exist only for certain parameter values.

Changing (fast) parameter values which occur only in the fast subsystem alter the active phase behavior [19] while changing (slow) parameter values which occur only in the slow subsystem can radically alter the global behavior of the solutions [21, 33, 34]. Here we discuss only those slow subsystem bifurcations needed in later sections.

Equilibria $\vec{u}_{ss} = (u_s, w_s, c_s)^T$ of (9)-(11) are those points represented in Figure 1 where the $\frac{dc}{dt} = 0$ nullcline intersects the $c = g(u)$ curve. Algebraically, u_s are roots of

$$\Delta(u) = g(u) - h(u) = -u^3 + (3-\beta)u + (\beta u_\beta + 3) \quad , \tag{37}$$

and $w_s = w_\infty(u_s), c_s = h(u_s)$. The cubic $\Delta(u)$ will have a single real root only if the discriminant

$$D_\Delta = \frac{1}{4}(\beta u_\beta + 3)^2 + \frac{1}{27}(\beta - 3)^3 \tag{38}$$

is positive. Solving $D_\Delta = 0$ we obtain two curves

$$u_\beta^\pm = \frac{1}{\beta}\left(-3 \pm \frac{2}{3\sqrt{3}}(3-\beta)^{3/2}\right) \quad , \quad \beta \leq 3 \quad , \tag{39}$$

which divides the $\vec{\lambda}_s = (\beta, u_\beta)$ slow parameter space into regions where (9)-(11) possesses one or three equilibria (cf. Figure 2). Between u_β^+ and u_β^-, Δ has three roots.

Next we determine the slow parameter values for which equilibria are lower ($u < u_m = -1$), middle ($u_m < u < u_M = 1$), or upper ($u > u_M$) branch. Middle branch equilibria will exist for $\vec{\lambda}_s$ lying between the curves $\Delta(u_m) = 0$ and $\Delta(u_M) = 0$. Solving the latter two equations, we obtain

$$u_\beta = u_\beta^m = -1 - 1/\beta \quad , \tag{40}$$

$$u_\beta = u_\beta^M = 1 - 5/\beta \quad . \tag{41}$$

For (β, u_β) between these two curves in Figure 2, at least one equilibria $\vec{u}_{ss}$ will be middle branch.

Next, we examine the stability of the equilibria. Linearizing (9)-(11) about $\vec{u}_{ss}$ yields the system

$$\vec{w}_t = D\mathbf{F}(\vec{u}_{ss})\vec{w} \quad , \tag{42}$$

with the jacobian

$$D\mathbf{F}(\vec{u}_{ss}) = \begin{bmatrix} f'(u_s) & -1 & -1 \\ w'_\infty(u_s) & -1 & 0 \\ \varepsilon h'(u_s) & 0 & -\varepsilon \end{bmatrix} \quad . \tag{43}$$

The characteristic polynomial $p(\lambda) = det(D\mathbf{F} - \lambda I)$ of (43) is

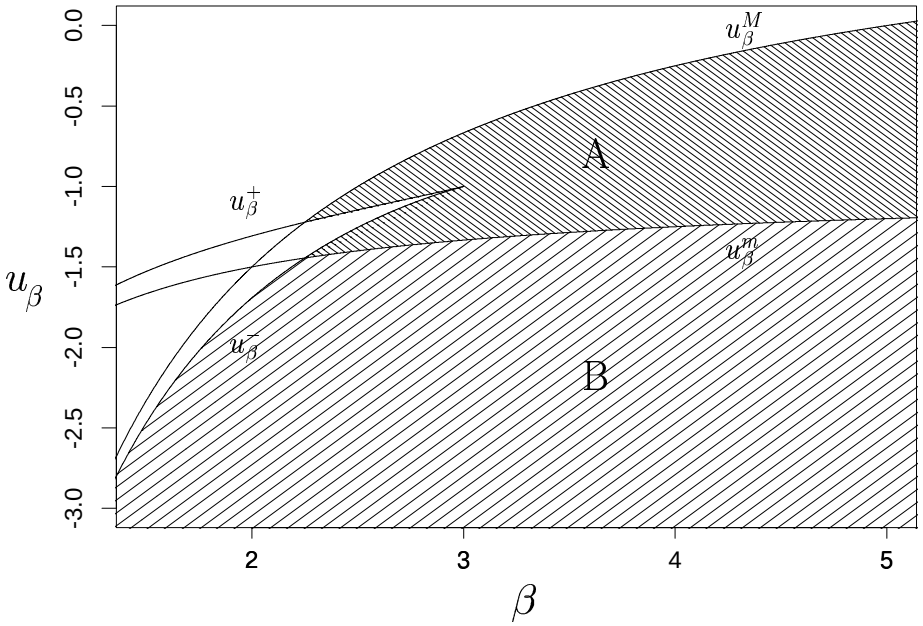

FIG. 2. *Dependence of equilibria on slow parameters. For (β, u_β) in region A, the single cell model possesses a single unstable equilibriium. In region B, the sole equilibrium is stable.*

$$p(\lambda) = -\lambda^3 + (f' - 1 - \varepsilon)\lambda^2 + (g' + \varepsilon(f' - 1 - h'))\lambda + \varepsilon(g' - h') \tag{44}$$

Since $0 < \varepsilon \ll 1$, two of the eigenvalues of (43) are asymptotic to those of the linearization of the fast subsystem (31)-(32) about $(u_s, w_s)^T$ with $c = c_s$. For instance, if $\vec{u}_{ss}$ intersects the lower branch of $c = g(u)$ in Figure 1, two eigenvalues of (43) have negative real parts since the corresponding fast subsystem equilibria are stable. If the intersection occurs on the middle branch (saddles), at least one eigenvalue of (43) will have positive real part implying $\vec{u}_{ss}$ is unstable.

The third eigenvalue of (43) can be estimated using the expansion

$$\lambda \sim \varepsilon\lambda_1 + \varepsilon^2\lambda_2 + \cdots \quad , \tag{45}$$

in (44) from which we obtain

$$\lambda_1 = \frac{h'(u_s)}{g'(u_s)} - 1 \quad . \tag{46}$$

If $\vec{u}_{ss}$ is middle branch, it is unstable from the previous arguments. If $\vec{u}_{ss}$ is lower branch, Figure 1 indicates that $g'(u_s) < 0$. For $h(u)$ defined in (17), $h'(u) = \beta > 0$. Therefore, for any (β, u_β) for which $\vec{u}_{ss}$ is lower branch, (46) implies $\lambda_1 < 0$ and $\vec{u}_{ss}$ is stable. Likewise, for any (β, u_β) for which $\vec{u}_{ss}$ is upper branch and (u_s, c_s) is a stable equilibria for the fast subsystem, $\vec{u}_{ss}$ is stable.

To summarize, for parameter values in region A of Figure 2, (9)-(11) has a sole unstable middle branch equilibria. For parameter values in region B, (9)-(11) has a sole stable lower branch equilibria. These two regions will distinguish active and inactive cells in section 8. We note here that for the parameter values (18), $\Delta(u_s) = 0$ has a single solution $u_s = -6/10$.

5. Nearest neighbour continuum models. In this section we introduce a continuum model for islet electrical activity for collections of cells whose dynamics are represented by the single cell model (9)-(11). We assume that cells are connected only to neighbouring cells resulting in the system:

$$\frac{\partial u}{\partial t} = f(u) - w - c + \nabla(D(x)\nabla u) \quad , \quad D \geq 0 \quad , \tag{47}$$

$$\frac{\partial w}{\partial t} = w_\infty(u) - w \quad , \tag{48}$$

$$\frac{\partial c}{\partial t} = \varepsilon(h(u) - c) \quad , \tag{49}$$

where $\phi = \phi(x,t)$ for $\phi = u, w, c$; $x \in \Omega \subset \mathbb{R}^3$, and $t > 0$. Cells on the boundary $\partial\Omega$ of the bounded domain Ω are not connected to any cells outside Ω by gap junctions. Thus, if $\hat{N}$ is the outward normal to $\partial\Omega$, the outward current flow $\mathbf{J} \cdot \hat{N} dS = -D\nabla u \cdot \hat{N} dS$ due to gap junctions through a surface element dS should vanish on the boundary making

$$\frac{\partial u}{\partial n} = \nabla u \cdot \hat{N}|_{\partial\Omega} = 0 \quad , \tag{50}$$

an appropriate boundary condition for the membrane potential u. Together with the initial conditions $\phi(x,0), \phi = u, w, c$, (47)-(50) defines the continuum model for islet electrical activity. The inclusion of a spatially-dependent D into a model reflects spatial inhomogeneity in the nearest neighbour coupling.

The connection between the continuum model (47)-(50) and its discrete counterpart can easily be demonstrated on a one dimensional string of cells. Here we let $x \in \Omega = [0, \ell]$ and D is a constant. First, define $u_i = u(x_i, t)$, $w_i = w(x_i, t)$, $c_i = c(x_i, t)$, where $x_i = i\Delta x$ is the location of the i-th cell ($i = 0, 1, 2 \ldots N$) in the string of $N+1$ cells so that the cell diameter $\Delta x = \ell/N$. Since we assume the number of cells is large, $\Delta x \ll 1$ and a first order discretization of the boundary conditions for u is

$$\frac{\partial u}{\partial x}(0,t) \simeq \frac{u_1(t) - u_0(t)}{\Delta x} = 0 \quad , \quad \frac{\partial u}{\partial x}(\ell,t) \simeq \frac{u_N(t) - u_{N-1}(t)}{\Delta x} = 0 \quad , \tag{51}$$

which imply

$$u_0(t) = u_1(t) \quad , \quad u_N(t) = u_{N-1}(t) \quad . \tag{52}$$

Using a second-order discretization of the diffusion term u_{xx} and (52) to simplify the endpoint equations yields the following discretization of (47):

$$\frac{du_0}{dt} = f(u_0) - w_0 - c_0 + \gamma\,(u_1 - u_0) \quad , \tag{53}$$

$$\frac{du_i}{dt} = f(u_i) - w_i - c_i + \gamma\,(u_{i+1} - 2u_i + u_{i-1}) \quad , i = 1, 2, \ldots N-1 \quad , \tag{54}$$

$$\frac{du_N}{dt} = f(u_N) - w_N - c_N + \gamma\,(u_{N-1} - u_N) \quad , \tag{55}$$

where

$$\gamma = \frac{D}{\Delta x^2} \quad . \tag{56}$$

The system (53)-(55) clearly represent the current balance equations for a string of $N+1$ cells with a fixed gap junction conductance of γ. If Δx is sufficiently small, the solution in (53)-(55) will accurately approximate $u(x,t)$. Conversely, if Δx is sufficiently small, $u(x_i,t)$ will accurately approximate $u_i(t)$.

6. Equilibria of the continuum model. In this section, we show that for slow parameter values taken from regions A or B in Figure 2 the continuum model possesses a sole spatially homogeneous equilibria whose stability matches that of those of the corresponding kinetic system (9)-(11) to leading order in ε. We first show equilibria are unique by using a comparison theorem. Stability will be demonstrated using standard linear analysis.

Equlilibria $\vec{U}(x) = (U(x), W(x), C(x))^T$ of the continuum model satisfy

$$\nabla(D(x)\nabla U) + \Delta(U) = 0 \quad , \quad \left.\frac{\partial U}{\partial n}\right|_{\partial\Omega} = 0 \quad , \tag{57}$$

$$W(x) = w_\infty(U(x)) \quad , \tag{58}$$

$$C(x) = h(U(x)) \quad . \tag{59}$$

where $\Delta(u)$ is defined in (37). The continuum model possesses a sole equlibria if and only if the scalar elliptic problem (57) does. The comparison theorem we use to show (57) has a unique equilibria is stated and proved in [32]. We restate it here without proof noting it is sufficient if all functions in the following definitions are C^2 in their arguments. First, we define the linear parabolic operator

$$P[u] = \sum_{i,j=1}^{3} (a_{ij}(x,t)u_{x_i})_{x_j} - u_t \quad , \tag{60}$$

$(x,t) \in R = \Omega \times (0,T)$, $u = u(x,t)$, and where a_{ij} is a symmetric positive definite matrix whose elements are bounded on R. Also, define the boundary operator

$$B[u] = \frac{du}{d\nu} + \alpha(x,t)u \quad , \quad \alpha \geq 0 \quad , \quad (x,t) \in \partial R, \tag{61}$$

where ν is any outward direction relative to ∂R.

THEOREM 1. *Suppose there are functions $u(x,t)$ and $v(x,t)$ such that*

a) $P[u] - \phi(x,t,u) \leq P[v] - \phi(x,t,v)$ *for* $(x,t) \in R$

b) $B[u] \geq B[v]$ *for* $(x,t) \in \partial R$

c) $u(x,0) = u_0(x) \geq v(x,0) = v_0(x)$ *for* $x \in \Omega$

then $u(x,t) \geq v(x,t)$ *for all* $(x,t) \in \bar{R}$.

In our application,

$$P[\psi] = \nabla(D(x)\nabla\psi) - \psi_t \quad , \tag{62}$$

$$B[\psi] = \frac{d\psi}{dn} \quad , \tag{63}$$

and $\phi(x,t,u) = -\Delta(u)$. Furthermore we use the theorem in the context where both left and right sides of hypotheses a)-b) equal zero, in which case, u and v are any solutions of the boundary value problem

$$P[\psi] + \Delta(\psi) = 0 \quad , \quad B[\psi] = 0 \quad , \quad \psi(x,0) = \psi_0(x) \quad . \tag{64}$$

Now let the upper solution $v^+(t)$ and the lower solution $v^-(t)$ satisfy the ordinary differential equations

$$\frac{dv^+}{dt} = \Delta(v^+) \quad , \quad v^+(0) = M \quad , \tag{65}$$

$$\frac{dv^-}{dt} = \Delta(v^-) \quad , \quad v^-(0) = m \quad . \tag{66}$$

For $(\beta, u_\beta) \in A \cup B$, $\Delta(u) > 0$ if $u < u_s$ and $\Delta(u) < 0$ if $u > u_s$. Therefore, for any choice of m, M with $m < u_s < M$, $v^+(t)$ and $v^-(t)$ monotonically decrease and increase to u_s , respectively, as $t \to \infty$. Since $v^\pm$ are also solutions of (64), Theorem 1 implies that for any solution $u(x,t)$ of (64) with $m \le u_0(x) \le M$,

$$v^-(t) \le u(x,t) \le v^+(t) \quad , \quad \forall (x,t) \in R \tag{67}$$

Taking the limit as $T \to \infty$, we see that $u(x,t) \to u_s$. Thus, u_s is the only stable equilibria of (64). To show that no other equilibria $U(x)$ can exist we merely choose m and M small and large enough so that $m < u_0(x) = U_s(x) < M$. Then, in the limit $T \to \infty$, the inequality (67) contradicts the supposition that $U(x) \neq u_s$ is an equilibria. Since equilibria of (64) are the solutions of (57), we conclude the continuum model possesses a sole equilibria for all (β, u_β) for which Δ has a sole root. Lastly, we note that these existence results applying in any spatial dimension ≤ 3 and for any $D(x) \ge 0$.

Now we demonstrate the stability of the equilibria of the continuum model matches that of the kinetic system (9)-(11). Linearizing (47)-(49) about $\vec{U} = (U, W, C) = (u_s, w_s, c_s)$ we obtain the system

$$\vec{w}_t = D\mathbf{F}(\vec{U})\vec{w} + \mathbf{L}[\vec{w}] \quad , \vec{w} = (\tilde{u}, \tilde{w}, \tilde{c})^T \tag{68}$$

where $\mathbf{L}[\vec{w}] = diag(\nabla(D(x)\nabla\tilde{u}), 0, 0) = diag(L[\tilde{u}], 0, 0)$ and $D\mathbf{F}$ is as given in (43). Seeking solutions of the form $\vec{w}(x,t) = e^{\lambda t}\vec{W}(x)$, we obtain the eigenvalue problem

$$L[\tilde{U}] + f'(U)\tilde{U} - \tilde{W} - \tilde{C} = \lambda\tilde{U} \quad , \tag{69}$$

$$w'_\infty(U)\tilde{U} - \tilde{W} = \lambda\tilde{W} \quad , \tag{70}$$

$$\varepsilon h'(U)\tilde{U} - \varepsilon\tilde{C} = \lambda\tilde{C} \quad , \tag{71}$$

for $\vec{W} = (\tilde{U}, \tilde{W}, \tilde{C})^T$, where $\lambda \neq -1, -\varepsilon$. Solving (70) and (71) for $\tilde{W}$ and $\tilde{C}$, respectively, and then substituting into (69) we obtain the scalar eigenvalue problem

$$L[\tilde{U}] = \mu(\lambda)\tilde{U} \quad , \tag{72}$$

$$\mu(\lambda) = \frac{w'_\infty(U)}{\lambda+1} + \frac{\varepsilon h'(U)}{\lambda+\varepsilon} + \lambda - f'(U) \quad , \tag{73}$$

for $\tilde{U}$ in which λ enters in a nonlinear way. It is well known that the eigenvalues μ_k of L with its associated Neumann boundary conditions are nonpositive and real, i.e., $0 \geq \mu_1 > \mu_2 \cdots$. Since U is constant, eigenvalues λ of (69)-(71) correspond to all those (complex) solutions of $\mu(\lambda_k) = \mu_k, k = 1, 2, \ldots$. Equivalently, λ are roots of the cubic

$$p(\lambda) = p_0(\lambda) + \varepsilon p_1(\lambda) \quad , \tag{74}$$

obtained from (73) where (using (13), (33), and $\bar{\tau} = 1$ to simplify the results)

$$p_0(\lambda) = \lambda(\lambda^2 + p_{01}\lambda + p_{00}) = \lambda(\lambda^2 + (F-\mu)\lambda - (g' + \mu)) \quad , \tag{75}$$

$$p_1(\lambda) = \lambda^2 + p_{11}\lambda + p_{10} = \lambda^2 + (F - \mu + h')\lambda - (g' + \mu - h') \quad . \tag{76}$$

Clearly, two roots $\lambda_\pm = O(1)$ while the remaining root $\bar{\lambda} = O(\varepsilon)$.

The equilibria will be stable if and only if the real part of $\lambda_\pm$ and $\bar{\lambda}$ are negative for all $\mu \leq 0$. Since the leading value of $\lambda_\pm$ is given as the solution of the quadratic factor of p_0, $\mathbb{R}e(\lambda_\pm) < 0$ if and only if both $p_{01} > 0$ and $p_{00} > 0$. Thus, $\mathbb{R}e(\lambda_\pm) < 0$ for all $\mu \leq 0$ if and only if

$$F(U) > 0 \quad , \tag{77}$$

$$g'(U) < 0 \quad . \tag{78}$$

Letting $\bar{\lambda} \sim \varepsilon\bar{\lambda}_0 + O(\varepsilon^2)$, we find from (74)-(76):

$$\bar{\lambda}_0 = \frac{h'}{g' + \mu} - 1 \quad . \tag{79}$$

Thus, $\mathbb{R}e(\bar{\lambda}) < 0$ if and only if

$$\frac{h'(U)}{g'(U) + \mu} < 1 \quad . \tag{80}$$

If (78) is satisfied, (80) will automatically be satisfied since $h'(U) = \beta > 0$. Thus, it sufficies to determine when (77)-(78) are satisified.

For $\vec{\lambda}_s \in A \cup B$, (78) is satisfied only if U is lower branch (i.e., $\vec{\lambda}_s \in B$). Also, for the model under consideration, square wave bursting can exist only if $F(U) > 0$ on the lower branch [19] [1]. Therefore, $\mathbb{R}e(\bar{\lambda}), \mathbb{R}e(\lambda_\pm) < 0$ for all $\mu \leq 0$ only if $\vec{\lambda}_s \in B$,

[1] else the lower branch of the kinetic system has an additional Hopf point

or u_s is lower branch. From these facts, we summarize that for $\vec{\lambda}_s \in A \cup B$, the continuum model has a sole spatially homogeneous equilibria $U(x) = u_s$. If $\vec{\lambda}_s \in B$, it is stable. If $\vec{\lambda}_s \in A$, it is unstable. These facts are true in all spatial dimensions ≤ 3 and for all $D(x) \geq 0$. In particular, for $\vec{\lambda}_s \in B$, no turing instabilities are present.

7. Fast and Slow Subsystems for $D = O(1/\varepsilon)$. In this section, we specialize our analysis to the case where $D = O(1/\varepsilon)$ uniformly on Ω where, for simplicity, we set $D(x) = \frac{1}{\varepsilon}\bar{D}(x)$. This case corresponds to synchrony of the bursting through large (spatially inhomogeneous) gap junction coupling. Our objective is to show that nonsynchronous behavior of the slow variables is possible even though fast variables are synchronized to leading-order. Thus, throughout this section, we consider the initial conditions

$$u(x,0) = \bar{u} \quad , \tag{81}$$

$$w(x,0) = \bar{w} \quad , \tag{82}$$

$$c(x,0) = \bar{c}(x) \quad , \quad x \in \Omega \quad , \tag{83}$$

where $\bar{u}$ and $\bar{w}$ are constants. Furthermore, we assume $||\nabla \bar{c}|| = O(1)$ uniformly on Ω to exclude the possibility of boundary or internal layers in $c(x,t)$.

For the fast subsystem, we assume the regular expansions

$$\phi(x,t) \sim \phi_0(x,t) + \varepsilon\phi_1(x,t) + \ldots \quad , \quad \phi = u, w, c \quad , \tag{84}$$

are valid for times $t = O(1)$. Substitution of (84) into (47)-(49) and (81)-(83) yields the leading-order problem

$$\nabla \cdot (\bar{D}(x)\nabla u_0) = 0 \quad , \quad u_0(x,0) = \bar{u} \quad , \tag{85}$$

$$w_{0,t} = w_\infty(u_0) - w_0 \quad , \quad w_0(x,0) = \bar{w} \quad , \tag{86}$$

$$c_{0,t} = 0 \quad , \quad c_0(x,0) = \bar{c}(x) \quad , \tag{87}$$

and the $O(\varepsilon)$ problem

$$u_{0,t} = f(u_0) - w_0 - c_0 + \nabla \cdot (\bar{D}(x)\nabla u_1) \quad , \quad u_1(x,0) = 0 \quad , \tag{88}$$

$$w_{1,t} = w'_\infty(u_0)u_1 - w_1 \quad , \quad w_1(x,0) = 0 \quad , \tag{89}$$

$$c_{1,t} = h(u_0) - c_0 \quad , \quad c_1(x,0) = 0 \quad , \tag{90}$$

with the boundary conditions

$$\frac{\partial u_i}{\partial n}|_\Omega = 0 \quad , \quad i = 0, 1 \quad . \tag{91}$$

Clearly, (85) and (91) imply $u_0 = u_0(t)$ where $u_0(0) = \bar{u}$. This dependence on (x,t) further implies, from (86), $w_0 = w_0(t)$ with $w_0(0) = \bar{w}$. Moreover, $c_0 = \bar{c}(x)$.

Introducing the average notation

$$< \phi(x,t) >= \hat{\phi}(t) = \frac{1}{|\Omega|}\int_{\Omega} \phi(x,t)dx \quad , \tag{92}$$

where $|\Omega|$ is the volume of Ω and $\phi(x,t)$ is any function, the average of (88) is

$$u_{0,t} = f(u_0) - w_0 - \hat{c}_0 + < \nabla \cdot (\bar{D}(x)\nabla u_1) > \quad . \tag{93}$$

Using the divergence theorem and the boundary conditions on u_1 to simplify (93), we obtain from (86),(87) and (93) the space-independent fast subsystem

$$u_{0,t} = f(u_0) - w_0 - \hat{c}_0 \quad , \tag{94}$$

$$w_{0,t} = w_\infty(u_0) - w_0 \quad , \tag{95}$$

$$c_0 = \bar{c}(x) \quad . \tag{96}$$

The fast subsystem (94)-(95) is a set of ordinary differential equations whose solution can be determined for any given set of initial conditions $(\bar{u}, \bar{w}, \bar{c}(x))$. Such solutions $u_0 \sim u$ uniformly on Ω for $t = O(1)$ only. Also, it should be noted that invariant sets of the single cell fast subsystem (31)-(32) are also solutions to (94)-(95). In particular, (94)-(95) admits stable periodic solutions providing $\hat{c}_0 \in (c_m, c_{HC})$. Moreover, bistability is retained in (94)-(95) for $\hat{c}_0 \in (c_m, c_{HC})$ (cf. Figure 1).

For the slow subsystem analysis, we introduce the slow time $\tilde{t} = \varepsilon t$ and assume the expansions

$$\phi(x,t) \sim \Phi_0(x,\tilde{t}) + \varepsilon\Phi_1(x,\tilde{t}) + \ldots \quad , \quad \phi = u, w, c \quad , \tag{97}$$

are valid for times $\tilde{t} = O(1)$. Substitution of (97) into (47)-(50) and (81)-(83) yields the leading-order problem

$$\nabla \cdot (\bar{D}(x)\nabla U_0) = 0 \quad , \quad U_0(x,0) = \bar{u} \quad , \tag{98}$$

$$W_0 = w_\infty(U_0) \quad , \quad W_0(x,0) = \bar{w} \quad , \tag{99}$$

$$C_{0,\tilde{t}} = h(U_0) - C_0 \quad , \quad C_0(x,0) = \bar{c}(x) \quad , \tag{100}$$

and the $O(\varepsilon)$ problem

$$\nabla \cdot (\bar{D}(x)\nabla U_1) = C_0 - g(U_0) \quad , \quad U_1(x,0) = 0 \quad , \tag{101}$$

$$W_{1,\tilde{t}} = w'_\infty(U_0)U_1 - W_1 \quad , \quad W_1(x,0) = 0 \quad , \tag{102}$$

$$C_{1,\tilde{t}} = h'(U_0)U_1 - C_1 \quad , \quad C_1(x,0) = 0 \quad , \tag{103}$$

with the boundary conditions

$$\frac{\partial U_i}{\partial n}|_\Omega = 0 \quad , \quad i = 0, 1 \quad . \tag{104}$$

Clearly (98) and (99) imply $U_0 = U_0(\tilde{t})$ and $W_0 = W_0(\tilde{t})$. Thus, averaging (100)-(101), applying the divergence theorem, and using the boundary condition for U_1, we obtain from (99)-(101) the spatially independent slow subsystem

$$\hat{C}_0 = g(U_0) \quad , \tag{105}$$

$$W_0 = w_\infty(U_0) \quad , \tag{106}$$

$$\frac{d\hat{C}_0}{d\tilde{t}} = h(U_0) - \hat{C}_0 \quad . \tag{107}$$

To determine the time dependence of U_0, first differentiate (105) in $\tilde{t}$ and then use (105)-(107) to eliminate $\hat{C}_0$:

$$\frac{dU_0}{d\tilde{t}} = \frac{h(U_0) - g(U_0)}{g'(U_0)} \quad . \tag{108}$$

For a given initial condition $(\bar{u}, \bar{w}, \bar{c}(x))$ which satisfies (105)-(106), $U_0(0) = \bar{u}$ is used as an initial condition in (108) to determine $U_0(\tilde{t})$. Using this solution in (100), we obtain

$$C_0(x,t) = e^{-\tilde{t}} \left(\bar{c}(x) + \int_0^{\tilde{t}} e^s h(U_0(s)) ds \right) \quad . \tag{109}$$

In this manner, explicit solutions to the slow subsystem are possible with $u(x,t) \sim U_0(\tilde{t})$ and $c(x,t) \sim C_0(x,\tilde{t})$ uniformly in x for $\tilde{t} = O(1)$.

The fast subsystem (94)-(96) and the slow subsystem (105)-(107) are the same as their single cell counterparts when c is replaced by its spatial average. Thus, the fast subsystem bifurcation analyses in [19] remain true if c is replaced by $\hat{c}$. In particular, the same fast parameter values $(a, \hat{u}, \eta)$ which give rise to square-wave bursting in the single cell model will give rise to spatially synchronized square-wave oscillations in the continuum model providing $\hat{c}$ has a value where that active phase analysis is applicable, i.e., $1 < \hat{c} < 5$ for the model defined in section 2. This means that local oscillations in the continuum model can occur even if $c(x,t)$ is larger (or smaller) than the value required for single cell's fast subsystem to maintain oscillations.

We illustrate this fact and nonsynchronous behavior of the slow variable c numerically by computing the solution of (47)-(49), (18)-(30) for $D = 100, \Omega = [0,1]$, in Figure 4. Initial conditions for the run were $(\bar{u}, \bar{w}, \bar{c}(x)) = (-2, 0, 1.3 - 0.4(arctan((x - 0.7)/\delta) - arctan((x - 0.5)/\delta)))$ with $\delta = 0.01$ [2]. The method of lines was employed using a Gear integrator in time $(0 \le t \le 200)$ and 50 spatial grid points per time step $(0 \le x \le 1, \Delta x = 0.02)$.

Firstly, in Figure 3 the numerical solution $(c(\bar{x},t), u(\bar{x},t)$ for $\bar{x} = 0.6$ is superimposed onto the fast susbsytem bifurcation diagram for a single cell. The figure clearly illustrates how u and c in the continuum model may lie outside the range of the fast-slow range in the single cell analysis. In particular, note that active phase oscillations persist beyond the homoclinic bifurcation of the single cell model and the silent phase is not close to the $G(u,c) = 0$ curve. However, the projection of the averaged trajectory $(\hat{c}, \hat{u})$ onto the same diagram yields a picture essentially identical to Figure 1 (not shown here).

[2] The initial condition $\bar{c}(x)$ was chosen to introduce a large pulse on the interval $(0.5, 0.7)$ where c attains a value near 2.4

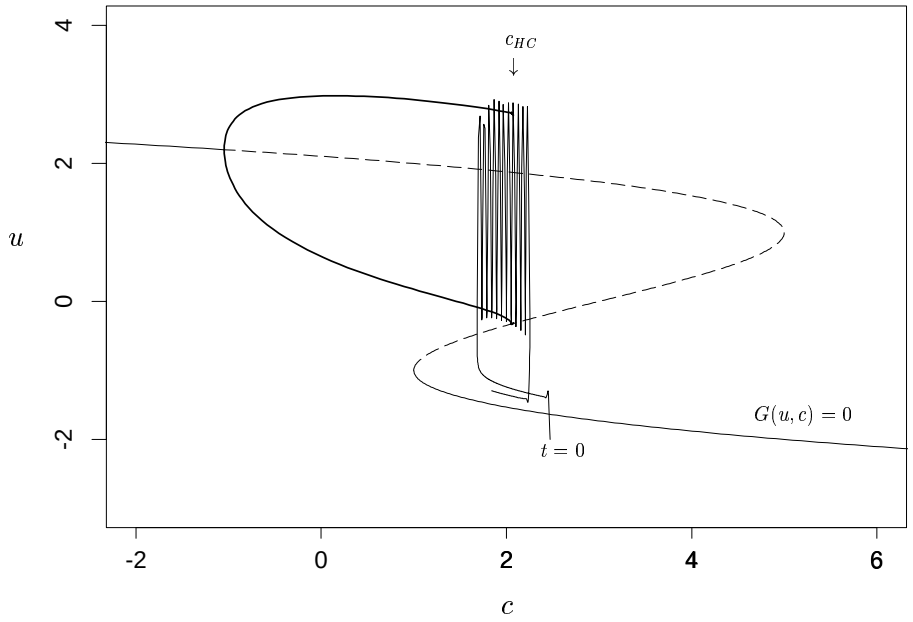

FIG. 3. *Projection of* $(c(\bar{x},t),u(\bar{x},t))$ *onto the single cell fast subsystem diagram for a fixed* $\bar{x}$. *Demonstrates how strong coupling induces individual cell activity significantly different than the single cell model.*

Figure 4a shows the synchronous behavior of $u(x,t)$. This is especially evident by the horizontal dark stripes indicating local maxima of the active phase oscillations. In contrast to the solution of Figure 4a, the solution of $c(x,t)$ illustrated in Figure 4b is nonsynchronous. In Figure 5, the nonsynchronous behavior of $c(x,t)$ is shown to diminish as $t \to \infty$ - a limiting case for which the fast and slow subsystem analysis presented in this section does not apply.

It should be emphasized that the theory presented in this section is applicable to islets $\Omega \subset \mathbb{R}^3$ and that only the numerics are in a one dimensional space domain. Also, the fast and slow subsystems developed here do not apply to all initial conditions. If, for example $\bar{u}$ were not constant, u_0 would have spatial dependence and (94) would no longer be valid.

8. Damaged Islet Model for $D = O(1/\varepsilon)$. In this section we introduce a model to simulate an islet which contains some fraction, ρ, of inactive cells which if uncoupled from the other cells exhibit stationary rather than bursting behavior. It will be demonstrated that for sufficiently large ρ, the entire islet no longer exhibits synchronous bursting and that c is lower on average than if no cells were inactive. Though, many of the ideas of this section are easily extended to domains of higher dimension, we restrict our attention to a domain $\Omega = [0,1]$ for simplicity.

In the model, we introduce an inhomogeneity in slow parameters which regulate the dynamics of c. Cells with slow parameters in region A of Figure 2 will be referred to as "active". Cells with slow parameters in region B will be referred to as "inactive". Inactive cells exhibit stationary behavior whereas active cells burst.

For fixed $\beta > 3$ (which we assume for the remainder of the section), the analysis of section 4 implies cells will be inactive if $u_\beta < u_\beta^m$. In the continuum model, we

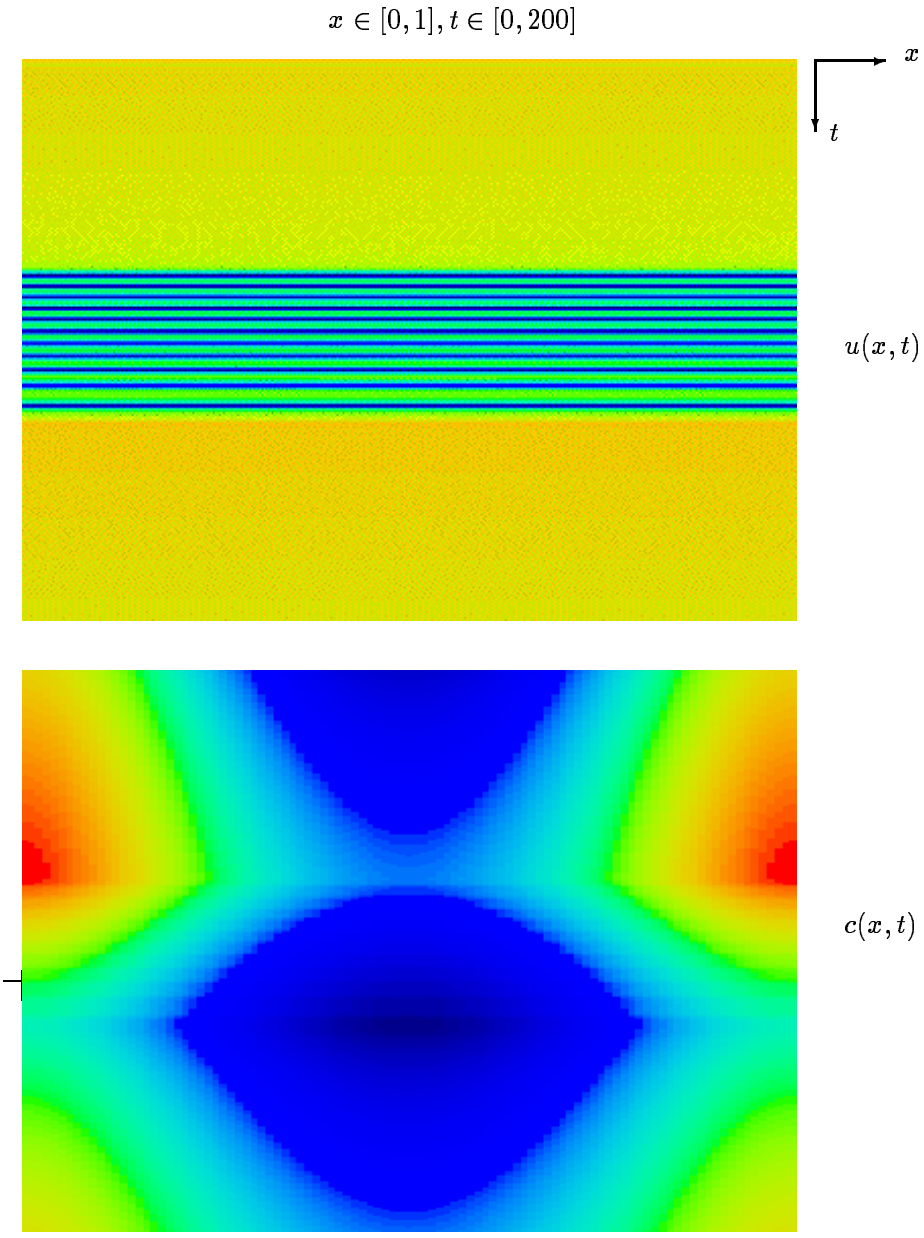

FIG. 4. *Numerical solution of a continuum model. Figures are greyscale contours with dark and light regions indicating higher and lower values of dependent variables, respectively. a) Shows synchronous bursting of* $u(x,t)$ *in* t *, b) Shows* $c(x,t)$ *is nonsynchronous.*

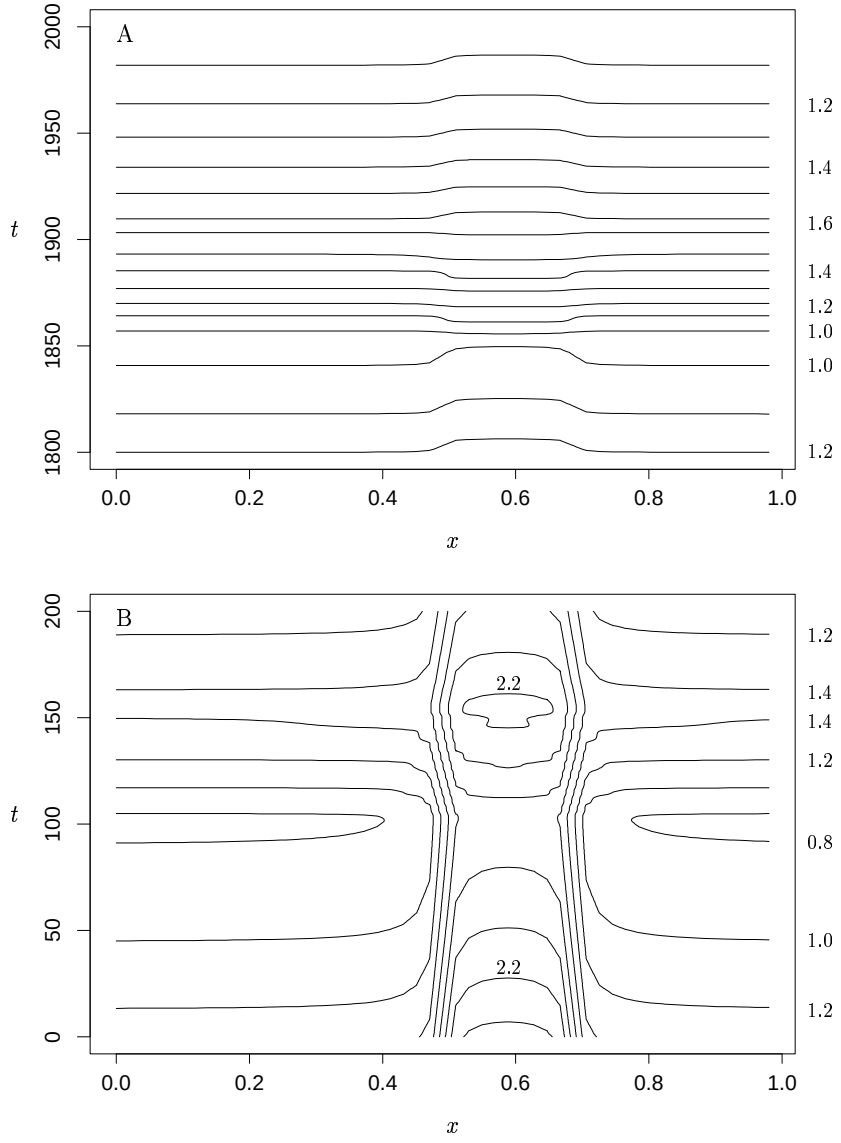

FIG. 5. *Long time numerical solution of continuum model. Figures are contours of $c(x,t)$ using same initial conditions as in Figure 4. Increments for contours (labelled on the right of each diagram) are 0.1 in b) and 0.2 in a). a) Shows that after a long time the slow variable $c(x,t)$ appears to synchronize whereas b) initially the behavior is highly nonsynchronous.*

model a inactive region in the islet by imposing a spatial dependence on u_β:

$$u_\beta(x) = u_+ - (u_+ - u_-)(H(x - x_0) - H(x - x_0 - \rho)) \quad , \tag{110}$$

where H is the Heaviside function and $u_\pm$ are constants. Letting $u_- < u_\beta^m < u_+ < u_\beta^M$, this spatial dependence in u_β introduces an interval $(x_0, x_0 + \rho)$ of inactive cells each with $u_\beta = u_-$ while the remaining fraction of cells, $1-\rho$, are active with $u_\beta = u_+$.

If we re-derive the slow subsystem (105)-(108) as in the previous section, we obtain

$$\frac{dU_0}{d\tilde{t}} = \frac{\hat{h}(U_0) - g(U_0)}{g'(U_0)} \tag{111}$$

$$\frac{d\hat{C}_0}{d\tilde{t}} = \hat{h}(U_0) - \hat{C}_0 = \hat{h}(U_0) - g(U_0) \quad , \tag{112}$$

where

$$\hat{h}(u) = \beta(u - \hat{u}_\beta) \quad , \tag{113}$$

$$\hat{u}_\beta = \int_0^1 u_\beta(x)dx = \rho u_- + (1-\rho)u_+ \quad . \tag{114}$$

The solution $(U_0(\tilde{t}), \hat{C}_0(\tilde{t}))$ determined by (111)-(112) is (for the same initial conditions) identical to the solution $(u(\tilde{t}), c(\tilde{t}))$ determined by (35)-(36) if $u_\beta = \hat{u}_\beta$. Since (35)-(36) has a sole stable (lower branch) equilibria if $u_\beta < u_\beta^m$, we conclude (111)-(112) has a sole (lower branch) stable equilibria if $\hat{u}_\beta < u_\beta^m$. Thus, using (114) and (40), if

$$\rho u_- + (1-\rho)u_+ < -\left(1 + \frac{1}{\beta}\right) \quad , \tag{115}$$

$(U_0, \hat{C}_0) \to (u_s, c_s)$ for lower branch initial conditions satisfying $\hat{C}_0 = g(U_0)$. Simplifying (115), we conclude that for

$$\rho > \rho^* = \frac{u_+ + 1 + 1/\beta}{u_+ - u_-} \quad , \tag{116}$$

(111)-(112) has a sole stable lower branch equilibria, (u_s, c_s). [1] Therefore, the asymptotic analysis predicts that if a large enough fraction of cells are inactive some solutions of (47)-(49) will have an average slow variable $\hat{c}(t) \to c_s$.

We confirm this numerically in Figure 6 where $(u(\bar{x}, t), \hat{c}(t))$ of an islet with $\rho = 0$ is compared to $(u_d(\bar{x}, t), \hat{c}_d(t))$ of an islet with $\rho > \rho^*$. The domain $\Omega = [0, 1]$ and initial conditions used for both computations were $(\bar{u}, \bar{w}, \bar{c}(x)) = (-2, 0, 1.2)$. As before, the method of lines with a Gear integrator was used with 50 spatial grid points per time step ($0 \le x \le 1, \Delta x = 0.02$). Additional parameter values used were: $x_0 = 0.5$,

[1] Furthermore, since (35)-(36) has no lower branch equilibria if $u_\beta > u_\beta^*$, (111)-(112) has no lower branch equilibria if $\rho < \rho^*$.

$\rho = 0.3, u_+ = u_\beta = -0.954, u_- = -2, D = 100$, and $\bar{x} = 0.5$. These values yield, for (116), $\rho > \rho^* = 0.283$.

Figure 6a shows a comparison of the bursting electrical activity in the islet with $\rho = 0$ and the stationary behavior in the islet with $\rho > \rho^*$. It is clear in Figure 6b that the average value $\hat{c}(t)$ is larger than $\hat{c}_d(t)$. This fact is especially important when c is interpretted as the intracellular calcium concentration since higher average levels of calcium are required for insulin secretion in the β-cell. When c is interpretted as intracellular calcium, the numerics confirm the asymptotic prediction that islet inhomogeneities can cause an islet average calcium $\hat{c}(t)$ to lower, subsequently inhibiting insulin secretion. These facts motivate the terminologies "damaged islet" and "undamaged islet" for $\rho > \rho^*$ and $\rho = 0$, respectively.

9. Discussion. In this paper, a systematic development of a continuum model for β-cell islet electrical activity has been presented. Two main goals of this work have been to 1) draw parallels between single cell models and the continuum model for large coupling strengths and 2) use a version of the continuum model to present a possible mechanism for diabetic conditions.

It is evident from the analysis presented in sections 3-7 that for strong coupling (large D) both the fast-slow subsystem equations and existence and stability of equilibria in the single cell and continuum models are similar. The spatial averaging used in section 7 demonstrated that the fast and slow susbsytems of the continuum model are the same as those of the single cell systems if slow variables are replaced by their spatial averages. This, in part, provides a formalization of the conjecture that single cell models represent average islet behavior. However, even if the coupling strength is large, the continuum model predicts that synchronous fast variable behavior can coexist (to leading-order) with nonsynchronous slow variable behavior. Since it is generally believed that slow variables (concentrations) are more directly connected to insulin production, this result suggests that islet electrical activity may not be a good measure for such production. For instance, if one assumes the production of insulin is connected to a threshold value of the slow variable c, the whole islet may exhibit synchronous electrical behavior even though some cells are not producing insulin. If further experimentation demonstrates weaker cell-cell coupling in the islet, such implications may not be true since the analysis applies only to strong coupling. Lastly, in Figure 5 it was shown that the short time nonsynchrony of the slow variable c does not persist on very long time scales. Though it was not explored here, an explanation of this phenomena may be possible by applying some of the shadow system theory developed by Hale and Sakamoto [11].

The equlibria analysis in sections 4 and 6 demonstrates that regardless of what the coupling strength is, coupling does not introduce any fundamentally new spatial patterning through equilibria bifurcations. The continuum model of section 5 possesses only those equlibria in the single cell model. Moreover, the stability of those equilibria is retained in the slow parameter space. Spatial patterning as a consequence of bifurcations in the periodic (bursting) solutions has not been excluded. This possiblity and the dependence of equilibria on parameter inhomogeneities have not been examined.

It is clear from the analysis in section 8, however, that islet inhomogeneities can have profound effects on average concentrations within the islet. What is particularly interesting from these results is that only a fraction of cells need be inactive to cause all bursting to cease and average concentrations to drop. Moreover, this result is

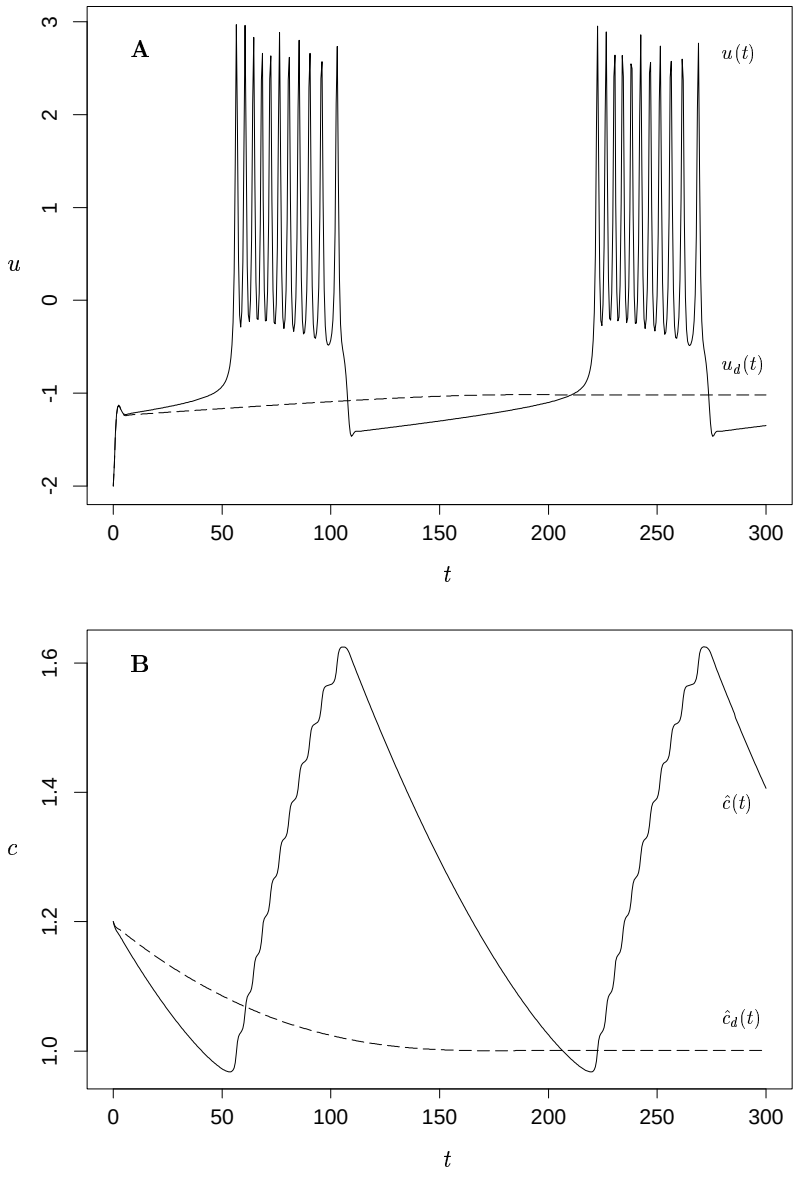

FIG. 6. *Numerical solutions of damaged and undamaged islet models. a) Shows a comparison of* $u(\bar{x},t)$ *and* $u_d(\bar{x},t)$. *b) Shows a comparison between the spatial averages of* $c(x,t)$. *Note that the average value of c in the damaged islet is lower than that of undamaged (bursting) islet.*

independent of the spatial distribution of $u_\beta(x)$. Again, if one assumes the production of insulin is connected to a threshold value of the slow variable c, this provides a possible mechanism for diabetic conditions. Should intracellular mechanisms which cause increases in the intracellular values of c be damaged through infection or other external factors, the whole islet could cease to produce insulin. Furthermore, in the continuum model, the fraction of inactive cells needed to cause this effect was less than 30 percent.

10. Acknowledments. This work has been was supported by the National Science Foundation grants OSR-93-50-546 and DMS-9404521. I would also like to extend my appreciation to Bard Ermentrout (U. Pittsburgh) for the development and distribution of his software "xtc" which facilitated much of the numerical work presented in this paper.

REFERENCES

[1] Beigelman, M., B. Ribalet, I. Atwater. 1977. Electrical activity of mouse pancreatic beta-cells: II Effects of glucose and arginine. *J. Physiol. (Paris)*. 73:201-217.

[2] Bertram, R., P. Smolen, A. Sherman, D. Mears, I. Atwater, F. Martin. 1995. A role for calcium release-activated current (CRAC) in cholinergic modulation of electrical activity in pancreatic β-cells. *Biophys. J.* 68:2323-2332.

[3] Chay, T.R., J. Keizer. 1985. Theory of the effect of extracellular potassium on oscillations in the pancreatic β-cell. *Biophys. J.* 48:815-827.

[4] Chay, T.R., D.L. Cook. 1988. Endogenous bursting patterns in excitable cells. *Math. Biosc.* 90:139-153.

[5] Chay T.R., H.S. Kang. 1987. Multiple oscillatory states and chaos in the endogenous activity of excitable cells: pancreatic β-cell as an example. In *Chaos in Biological Systems*. H. Degn, A.V. Holden, and L.F. Olsen, editors. Plenum Press. 173-181.

[6] Dean, P.M., E.K. Matthews. 1970a. Glucose-induced electrical activity in pancreatic islet cells. *J. Physiol. (Lond.)*. 210:255-264.

[7] Dean, P.M., E.K. Matthews. 1970b. Electrical activity in pancreatic islet cells: effects of ions. *J. Physiol. (Lond.)*. 210:265-275.

[8] G. de Vries, R.M. Miura, M. Pernarowski, Parameter studies for an analog model of bursting electrical activity. In *Differential Equations and Applications to Biology and Industry*, edited by M. Martelli, K. Cooke, E. Cumberbatch, B. Tang, and H. Thieme, World Scientific, Singapore, 1996, pp. 385-392.

[9] Doedel, E. J., AUTO: A program for the automatic bifurcation and analysis of autonomous systems, in *Proc. 10th Manitoba Conf. on Numer. Math. and Comput.*, Winnepeg, Canada, Congr. Numer., 30 (1981) pp. 265-284.

[10] Falke, L.C., K.D. Gillis, D.M. Pressel, S. Misler. 1989. Perforated patch recording allows long-term monitoring of metabolite-induced electrical activity and voltage-dependent Ca^{2+} currents in pancreatic B cells. *FEBS (Fed. Eur. Biochem. Soc.) Lett.* 251:167-172.

[11] Hale, J.K., K. Sakamoto. 1989. Shadow systems and attractors in reaction-diffusion equations. *Applicable Analysis* 32:287-303.

[12] Himmel, D.M., T.R. Chay. 1987. Theoretical studies on the electrical activity of pancreatic β-cells as a function of glucose. *Biophys. J.* 51:89-107.

[13] Keener, J. P. 1987 Propagation and its failure in coupled systems of discrete excitable cells. *SIAM J. Appl. Math.* 47:556-572.

[14] Meda, P., I. Atwater, A. Goncalves, A. Bangham, L. Orci, E. Rojas. 1984. The topography of electrical synchrony among B-cells in the mouse islets of Langerhans. *Q. J. Exp. Physiol.* 69:719-735.

[15] Meissner, H.P. 1976. Electrophysiological evidence for coupling between β-cells of pancreatuic islets. *Nature (Lond.)* 262:502-504.

[16] Meissner, H.P., H. Schmelz. 1974. Membrane potential of beta-cells in pancreatic islets. *Pflüegers Arch.* 351:195-206.

[17] Moser, J, Stable and Random Motions in Dynamical Systems, Princeton Univ. Press, Princeton, 1973.

[18] Perez-Armendariz,M., C. Roy, D.C. Spray, M.V.L. Bennett. 1991. Biophysical properties of gap junctions between freshly dispersed pairs of mouse pancreatic beta cells. *Biophys. J.* 59:76-92.

[19] Pernarowski, M. 1994. Fast subsystem bifurcations in a slowly varying Lienard system exhibiting bursting. *SIAM J. Appl. Math.* 54:814-832.

[20] Pernarowski, M., R.M. Miura, J. Kevorkian. 1991. The Sherman-Rinzel-Keizer model for bursting electrical activity in the pancreatic β-cell. *In* Differential Equation Models in Population Dynamics and Physiology. S. Busenberg and M. Martelli, editors. Springer-Verlag, Berlin. 34-53.

[21] Pernarowski, M., R.M. Miura, J. Kevorkian, J. 1992. Perturbation techniques for models of bursting electrical activity in pancreatic β-cells. *SIAM J. Appl. Math.* 52:1627-1650.

[22] Rinzel, J., T.R. Chay, D. Himmel, I. Atwater. 1986. Prediction of the glucose-induced changes in membrane ionic permeability and cytosolic Ca^{2+} by mathematical modelling. *Adv. Exp. Med. Biol.* 211:247-263.

[23] Rinzel, J. 1987. A formal classification of bursting mechanisms in excitable systems. *In* Mathematical Topics in Population Biology, Morphogenesis, and Neurosciences. E. Teramato and M. Yamaguti, editors. Springer-Verlag, Berlin. 267-281.

[24] Rorsman, P., G. Trube. 1986. Calcium and delayed potassium currents in mouse pancreatic β-cells under voltage-clamp conditions. *J. Physiol. (Lond.).* 374:531-550.

[25] Sattinger, D.H. 1972. Monotone methods in nonlinear elliptic and parabolic boundary value problems. *Ind. U. Math. J.* 21:979-1000.

[26] Sherman, A. 1994. Anti-phase, asymmetric and aperiodic oscillations in excitable cells - I. Coupled bursters. *Bull. Math. Biol.* 56:811-836.

[27] Sherman, A., J. Rinzel. 1991. Model for synchronization of pancreatic β-cells by gap junction coupling. *Biophys. J.* 59:547-559.

[28] Sherman, A., J. Rinzel. 1992. Rhythmogenic effects of weak electrotonic coupling in neuronal models. *Proc. Natl. Acad. Sci.* 89:2471-2474.

[29] Sherman, A., J. Rinzel, J. Keizer. 1988. Emergence of organized bursting in clusters of pancreatic β-cells by channel sharing. *Biophys. J.* 54:411-425.

[30] Smith, P.A., F.M. Aschroft, P. Rorsman. 1990. Simultaneous recordings of glucose dependent electrical activity and ATP-regulated K^+-currents in isolated mouse pancreatic β-cells. *FEBS (Fed. Eur. Biochem. Soc.) Lett.* 261:187-190.

[31] Smolen, P., J. Rinzel, A. Sherman. 1992 Why pancreatic islets burst but single β-cells do not: The heterogeneity hypothesis. *pre-print*

[32] Smoller, J., Shock Waves and Reaction-Diffusion Equations, 2nd ed., Springer-Verlag, 1994.

[33] Terman, D. 1991. Chaotic spikes arising from a model of bursting in excitable membrane. *SIAM J. Appl. Math.* 51:1418-1450.

[34] Terman, D. 1992. The transition from bursting to continuous spiking in excitable membrane models. *J. Nonlinear Sci.* 2:135-182.